Eur. Phys. J. A 10, 275–287 (2001)

THE EUROPEAN PHYSICAL JOURNAL A

Yrast level structure of the neutron-deficient N = 80 isotones ^{146}Dy, ^{147}Ho and ^{148}Er up to high-spin values

H.A. Roth[1,a], S.E. Arnell[1,†], D. Foltescu[1], Ö. Skeppstedt[1], J. Blomqvist[2], G. de Angelis[3], D. Bazzacco[4], and S. Lunardi[4]

[1] Department of Physics, Chalmers University of Technology, and the University of Gothenburg, S-41296 Göteborg, Sweden
[2] Department of Physics, The Royal Institute of Technology, S-10405 Stockholm, Sweden
[3] Istituto Nazionale di Fisica Nucleare, Laboratori Nazionali di Legnaro, I-35020 Legnaro, Italy
[4] Dipartimento di Fisica dell'Università, and Istituto Nazionale di Fisica Nucleare, Sezione di Padova, I-35131 Padova, Italy

Received: 12 January 2001 / Revised version: 10 April 2001
Communicated by D. Schwalm

Abstract. High-spin level schemes of the $N = 80$ isotones ^{146}Dy, ^{147}Ho and ^{148}Er have been investigated by in-beam γ-ray spectroscopic methods using the NORDBALL Compton-suppressed multidetector array including proton and neutron selection. The projectile-target system ^{58}Ni + ^{92}Mo at 260 MeV beam energy has been used to produce the neutron-deficient $N = 80$ isotones. The previously known schemes have been extended to considerably higher spin and exitation energy, up to $I = 23\hbar$, $E_x \approx 8.9$ MeV in ^{146}Dy, $I = 53/2\hbar$, $E_x \approx 8.7$ MeV in ^{147}Ho and $I = 23\hbar$, $E_x \approx 9.6$ MeV in ^{148}Er. The results are discussed in terms of the spherical shell model. Many of the levels can be described within this framework.

PACS. 23.20.Lv γ transitions and level energies – 25.70.Jj Fusion and fusion-fission reactions – 21.60.Cs Shell model – 27.60.+j $90 \leq A \leq 149$

1 Introduction

The ^{58}Ni + ^{92}Mo reaction at high energy gives a unique opportunity to study the yrast structure of a number of very proton-rich rare-earth nuclei in the neutron region $78 \leq N \leq 80$. These nuclei are positioned in a transition region just above the $Z = 64$, $N = 82$ nucleus ^{146}Gd, an almost doubly magic nucleus [1]. The nuclear structure of these nuclei will change rapidly with neutron number and the lighter isotones are expected to show how deformation sets in below the $N = 82$ shell closure.

In the present paper the yrast properties of the three $N = 80$ isotones ^{146}Dy, ^{147}Ho and ^{148}Er are studied. Up to the present work the following experimental information was available on the $N = 80$ isotones mentioned above.

^{146}Dy: A 150 ms 10^+ isomer was identified in ^{146}Dy by Gui *et al.* [2] and the decay of this isomer was studied both in-beam and in the β-decay of ^{146}Ho. A number of high-spin states above the 10^+ isomer has been identified by de Angelis *et al.* [3] by γ recoil and $\gamma\gamma$ coincidences.

^{147}Ho: A tentative level scheme of ^{147}Ho was obtained by Nolte *et al.* [4] in a bunched-beam experiment. Four γ-rays were observed, three of which decayed with a half-life of 315 ns. This half-life was attributed to the decay of an isomeric $27/2^-$ state. A missing $27/2^- \rightarrow 23/2^-$ $E2$ transition could, however, not be found. It was suggested that the missing transition should be strongly converted and have an energy less than 60 keV, since no strong K X-ray radiation was observed in coincidence with the γ transition de-exciting the $23/2^-$ level.

^{148}Er: Also this nucleus was studied by Nolte *et al.* [4] in a bunched-beam experiment. From $\gamma\gamma$ coincidences a decay scheme with about ten transitions could be established and with all levels decaying with a half-life of 13μs with respect to the pulsed beam. The half-life was attributed to the decay of an isomeric 10^+ state. Some γ transitions in ^{148}Er are also known from the β-decay of ^{148}Tm [5].

2 Experimental procedures

The isotones ^{146}Dy, ^{147}Ho and ^{148}Er were produced by the ^{58}Ni + ^{92}Mo reaction at $E(^{58}\text{Ni}) = 260$ MeV using a 10 mg/cm^2 ^{92}Mo target (^{92}Mo enrichment 98.37%). About 30×10^6 events were recorded. According to a CASCADE calculation at $E(^{58}\text{Ni}) = 260$ MeV [6], 2 mb of the total cross-section of 430 mb ($l_{\max} \approx 61\hbar$) constituted the 2p reaction channel leading to ^{148}Er, 104 mb the 3p channel leading to ^{147}Ho and 46 mb the 4p channel leading to ^{146}Dy. The integrated yields in percent of the total thick

[a] e-mail: halina.roth@fy.chalmers.se

target yield are 5% (2p), 32% (3p) and 8% (4p) from the CASCADE calculations. The particle beams, having intensities of the order of 1 particle nA, were delivered by the tandem booster accelerator at NBI Risø, Denmark. The γ-rays were detected in 15 BGO-shielded HPGe detectors situated in three rings of the NORDBALL frame [7] at 79°, 101° and 143° relative to the beam direction. The detectors were energy and efficiency calibrated with ^{56}Co, ^{152}Eu and ^{133}Ba sources.

The present investigation was performed at high projectile energy in order to enhance high-spin states and get large yields from a number of residual nuclei. This means that we had to use a very efficient particle selection system [8] in order to detect the large number of outgoing particle combinations (17 exit channels with cross-sections $\geq$1 mb). The system was adapted for spectroscopy of nuclei far from stability in the following way: In the forward hemisphere 11 liquid scintillator detectors formed a "neutron wall" [9]. Evaporated protons and α-particles were detected by a 4π Si ball consisting of 21 detectors [10]. At least two Compton suppressed γ-rays had to be detected within $\approx$ 100 ns in the Ge detectors together with at least one charged particle in the Si ball in order to generate a valid trigger and subsequently read out and store the events on 8 mm EXABYTE tapes. The γ-ray energy range covered is from 40 to 4000 keV. A more detailed account of the selection of reaction channels was given in a preceding article [11].

3 Data reduction

The general procedure of finding a clear $\gamma\gamma$-coincidence matrix for a certain residual nucleus starts by setting a gate in the particle identification spectrum for the channel in question with the neutron condition included, if appropriate. The "raw" matrix obtained in this way still contains "leaks" from reaction channels with larger particle multiplicities. These leaks are mainly due to the limited solid angle of the particle detectors. The raw matrix is cleaned by subtracting appropriate fractions of the matrices gated by larger numbers of detected particles. This requires a good knowledge of the projected spectra from all channels of higher multiplicity. The subtraction procedure is performed by a trial and error method.

The "raw" $\gamma\gamma$-coincidence matrices obtained by sorting all events associated with the 4p(^{146}Dy), 3p(^{147}Ho) and 2p(^{148}Er) emissions were corrected for contributions from reaction channels of higher proton multiplicities, from contributing xpn channels as well as channels containing one or two α-particles.

In the construction of the level schemes, the γ-rays were placed in the scheme by use of $\gamma\gamma$-coincidence relations and γ-ray intensities. Primarily, the intensities were obtained by summing the gain-shifted and efficiency-corrected contributions from the rings at 101° and 143°. The angles of the rings justify this procedure irrespective of the A2 coefficient of the angular distribution (the A4 coefficient is negligible in this context). The computer program ESCL8R [12] was used for control of the level schemes. This program allows fast and easy inspection and fitting of the peaks in the $\gamma\gamma$-coincidence matrix and is used to construct coincidence spectra based on assumed decay patterns, which are then compared to the observed spectra. In this way the program works backwards from the proposed level scheme, and attempts to reproduce the observed $\gamma\gamma$-coincidence matrix.

Information on the γ anisotropies was extracted from projected spectra recorded at 79°, 101° and 143° with respect to the beam axis. The assignment of level spins was mostly based on these anisotropies, defined as $R = 2I(143°)/[I(79°) + I(101°)]$. Considering the high angular momentum brought into the compound system, we assume that essentially all observed transitions have $J_i \geq J_f$ and most transitions have $J_i > J_f$. Crossover transitions are generally expected to be of $E2$ character.

4 Experimental results

4.1 Results for ^{146}Dy

The level scheme of ^{146}Dy deduced from the present work is displayed in figs. 1 and 2. Figure 3 shows some coincidence spectra and table 1 gives the γ-ray energies, relative intensities, anisotropies, and the placement of the transitions in the proposed level scheme. A plot of some R-values is given in fig. 4.

The level scheme shows a large number of new energy levels and has generally a complex and irregular structure especially at high excitation energy and numerous cross connections occur between the levels. The agreement with the part of the level scheme published by de Angelis *et al.* [3] is complete as regards the prompt or almost prompt γ-rays (the decay of the 10$^+$, 150 ms isomeric

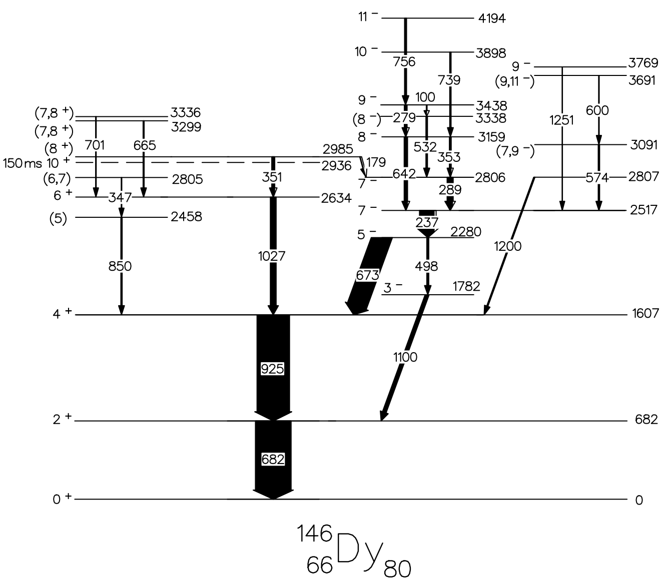

Fig. 1. Low-energy part of the level scheme of ^{146}Dy deduced from the present work. The widths of the arrows are roughly proportional to the relative γ-ray intensities. Energies are given in keV.

Table 1. Gamma-ray energies, intensities and anisotropy ratios for γ-ray transitions in ^{146}Dy.

E_γ (keV)	I_γ	R	I_i^π ($\hbar$)	I_f^π ($\hbar$)	E_γ (keV)	I_γ	R	I_i^π ($\hbar$)	I_f^π ($\hbar$)
68.6(3)	5(1)	0.9(1)	16_3^-	15_2^+	483.5(4)	7(1)	1.3(2)	15_1^-	13_1^-
100.5(3)	2(1)		9_1^-	(8^-)	498.1(3)	6(1)	2.0(4)	5^-	3^-
117.5(5)	4(1)	1.2(3)	14_2^+	13_2^+	514.1(2)	12(2)	0.77(8)	16_2^-	15_2^-
133.3(4)	6(1)	0.5(1)	16_3^-	15_1^+	517.1(2)	16(3)	0.44(5)	17_1^-	16_1^-
145.4(3)	5(1)	0.6(1)	19_2^-	18_5^-	531.6(4)	7(2)	1.2(2)	(8^-)	7_2^-
149.1(3)	14(2)	0.71(7)	15_2^-	14_2^-	534.5(5)	5(1)	1.3(3)	18_1^-	16_2^-
163.5(3)	8(2)	1.0(1)	14_1^-	13_1^-	538.9(1)[a]	90(14)	1.56(6)	14_1^-	12^-
173.8(2)	10(2)	0.68(7)	15_3^-	14_2^+	539.5(6)[a]			15,16	14_2^-
178.3(3)[a]				16_1^-	550.1(5)	6(1)	0.8(1)	18_4^-	17_4^-
178.8(3)[a]	8(1)	0.65(8)	(8^+)	7_2^-	573.5(4)	8(1)	1.4(2)	$(7,9^-)$	7_1^-
201.9(2)	9(2)	0.6(1)	21_1^-	20_1^-	592.5(4)	5(1)	0.6(1)	13_2^-	12^-
203.8(3)	7(1)	0.59(16)	14_2^-	13_2^-	600.2(4)	8(2)	1.4(2)	$(9,11^-)$	$(7,9^-)$
209.5(3)[a]			17_2^-	16_3^-	632.4(2)[a]	7(2)	1.3(2)	11_2^-	11^+
209.8(3)[a]	40(6)	0.71(4)	12^-	11_2^-	633.4(3)[a]			$(16)_2$	15_3^-
223.2(5)	2(1)		14_2^+	14_1^+	642.0(2)	13(3)	0.82(9)	8^-	7_1^-
231.6(2)	17(3)	0.69(5)	17_2^-	16^+	665.0(4)	6(1)		$(7,8^+)_1$	6^+
234.1(2)	17(3)	0.77(6)	19_3^-	18_4^-	673.5(1)	57(9)	0.99(4)	5^-	4^+
236.4(3)[a]			11_2^-	12^+	682.5(2)	85(13)	1.45(5)	2^+	0^+
236.7(3)[a]	44(7)	1.35(6)	7_1^-	5^-	695.9(1)	65(10)	0.42(2)	11^+	10^+
239.7(3)	13(2)	0.89(8)	20_1^-	19_3^-	700.9(2)[a]	13(2)	1.1(1)	19_2^-	18_3^-
251.9(3)[a]			$(16)_1$	15_4^-	701.3(3)[a]			$(7,8^+)_2$	6^+
252.3(3)[a]	11(2)	0.66(7)	18_2^-	17_2^-	703.6(3)	1(1)		18_4^+	17^+
252.6(3)[a]			$(16)_2$	16_2^-	712.3(3)	6(1)	0.7(1)	15_1^+	14_2^-
257.5(2)	8(1)	1.6(2)	14_2^-	14_1^-	727.4(4)	5(1)		$(19)^-$	17_4^-
264.7(2)	4(1)	0.7(2)	19^+	18_2^+	730.5(4)	5(1)		16_1^-	14_1^-
267.5(2)	13(2)	0.73(8)	21_2^-	20_2^-	738.6(2)	6(1)	1.6(2)	10^-	8^-
278.6(2)	11(2)	0.61(9)	9_1^-	8^-	755.7(3)	13(3)	1.5(1)	11_1^-	9_1^-
289.0(2)	19(3)	1.4(1)	7_2^-	7_1^-	760.3(3)	17(3)	1.07(9)	16^+	15_1^-
295.6(3)	5(1)	0.7(1)	19^+	18_1^+	783.1(4)	8(1)	0.72(7)	16_3^-	15_1^-
316.4(4)	4(1)	1.7(4)	14_3^-	14_1^-	821.5(3)[a]	27(1)	0.91(6)	13_1^-	12^+
320.1(1)	31(5)	0.48(3)	15_1^-	14_1^-	822.4(4)[a]			13_1^+	12^+
323.7(1)	14(2)	0.71(6)	16_1^-	15_2^-	842.2(2)	28(4)	0.96(7)	12^-	11^+
329.8(3)	7(1)	0.80(7)	18_1^+	17^+	850.5(3)	4(1)		(5)	4^+
337.7(3)	2(1)		$(19)^+$	18_2^+	925.1(1)	79(12)	1.35(5)	4^+	2^+
346.8(4)	2(1)		(6,7)	(5)	938.7(2)	14(2)	1.4(1)	16^+	14_1^+
350.9(2)	8(1)		(8^+)	6^+	1008.4(5)	4(1)	0.8(2)	18_4^-	17_1^-
352.5(2)	9(2)		8^-	7_2^-	1027.0(3)	17(3)	1.5(1)	6^+	4^+
360.5(2)	15(3)	0.9(1)	18_2^+	17^+	1083.8(5)	2(1)		18_4^-	$(16)_2$
366.5(3)[a]	13(2)	0.66(8)	20_2^-	19_2^-	1092.1(1)	100(15)	1.44(4)	12^+	10^+
368.4(3)[a]			$(19)^+$	18_1^+	1100.5(3)	7(2)	0.9(1)	3^-	2^+
375.5(2)[a]	21(2)	0.90(7)	13_1^-	12^-	1127.3(3)	31(5)	1.33(8)	14_1^+	12^+
377.5(4)[a]			23^-	22^-	1132.5(4)	3(1)	1.2(3)	15_1^+	13_1^+
395.7(5)	21(3)	0.63(5)	12^+	11^+	1167.4(4)	6(1)	1.4(2)	17_4^-	15_3^-
397.5(5)[a]			15_3^-	14_1^+	1196.9(4)	5(1)	1.5(2)	15_2^+	13_1^+
398.5(5)[a]	20(3)	0.62(5)	18_3^-	17_2^-	1199.6(5)	3(3)			4^+
403.8(4)	4(1)	0.5(1)	15_4^-	14_3^-	1218.5(4)	11(2)	1.8(2)	13_1^+	11^+
406.3(1)	26(4)	0.80(5)	15_2^-	14_1^-	1233.5(6)	3(1)		13_2^+	12^+
409.8(2)	13(2)	0.41(5)	16_1^-	15_1^-	1251.2(5)	3(1)	1.2(2)	9_2^-	7_1^-
420.9(3)	11(2)	0.9(1)	14_2^-	13_1^-	1328.5(2)	26(4)	0.77(5)	11_2^-	10^+
438.2(5)	5(1)	0.9(3)	17_3^-	16_2^-	1350.3(3)	7(1)	1.2(2)	14_2^+	12^+
446.0(1)	53(5)	1.63(7)	12^-	12^+	1537.7(4)	5(1)	1.1(2)	18_5^-	16_1^-
450.8(4)	9(1)	0.60(8)	22^-	21_2^-	1628.5(6)	1(1)		13_2^+	11^+
459.5(2)	5(1)	0.4(1)	19_1^-	18_2^-	1831.6(9)	1(1)		14_3^+	12^+
470.4(2)	17(3)	0.75(9)	17^+	16^+					

[a] Not resolved

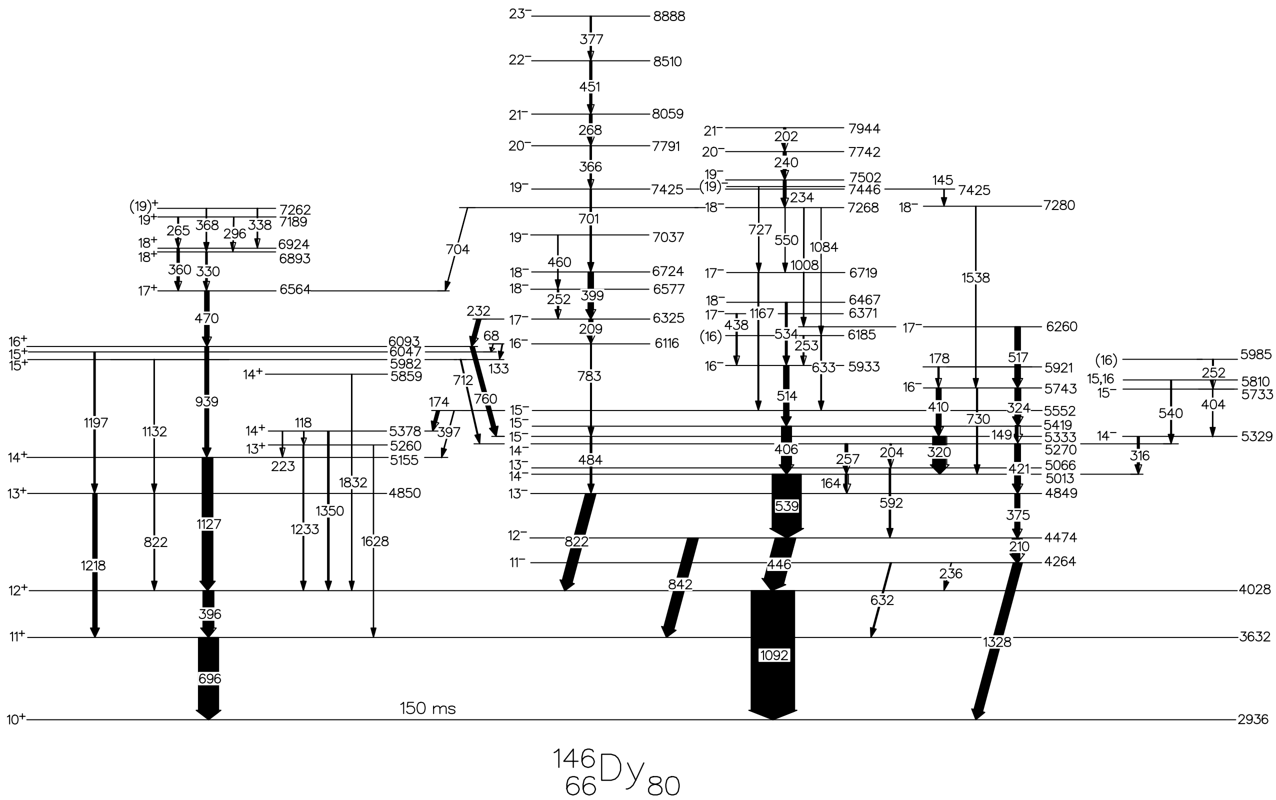

Fig. 2. High-energy part of the level scheme of ^{146}Dy deduced from the present work. This part shows the γ-decay to the 10^+, 150 ms isomeric state at 2935.6 keV [2]. The widths of the arrows are roughly proportional to the relative γ-ray intensities. Energies are given in keV.

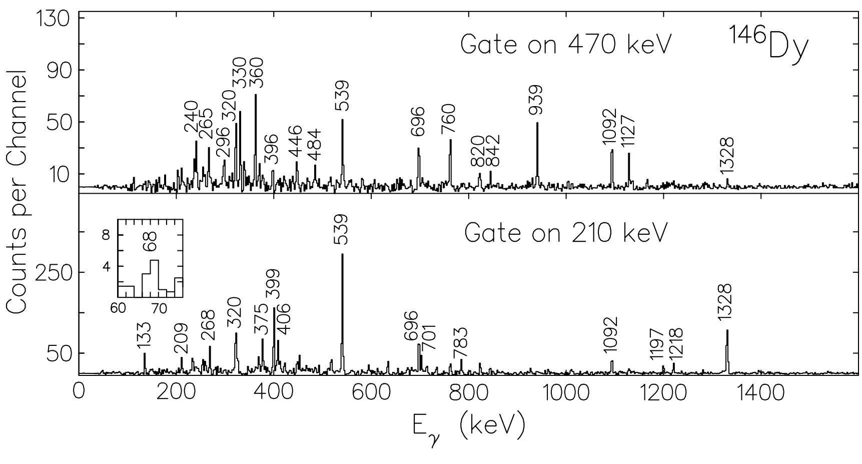

Fig. 3. Some background-subtracted $\gamma\gamma$-coincidence spectra of ^{146}Dy recorded with NORDBALL. Only the most prominent γ-rays are indicated. Note that the 210 keV gating transition is a doublet ($17^- \rightarrow 16^-$ and $12^- \rightarrow 11^-$).

state was not studied in the present work).

The decay scheme, as observed in the present investigation, can be separated in two parts, one part (fig. 1) representing states at relatively low excitation energy ($\leq$ 4.2 MeV) and with low spin values ($\leq 11\ \hbar$). All these states have a prompt decay to the ground state. The other part of the decay scheme (fig. 2) extends to high excitation energy ($\approx$ 8.9 MeV) and to the spin value of 23 $\hbar$. These states de-excite to the 10^+, 150 ms isomeric state at 2936 keV.

The first part of the scheme (fig. 1) shows, besides a few transitions between low-lying positive-parity states, a side structure of parallel cascades of negative parity de-excited by $E1$ transitions to the 2^+ and 4^+ yrast states. In the second part (fig. 2) of the level scheme the three strong 1092, 1127 and 939 keV stretched $E2$ transitions form a cascade from the isomeric 10^+ level up to the 6093 keV, 16^+ state. Above the 12^+ state at 4028 keV a side structure of negative-parity develops.

The 209 keV line de-exciting the level at 6325 keV has a well established coincidence relationship with the 1197–1218 keV cascade to the 11^+ level at 3632 keV (fig. 2). There is an energy gap of 68 keV and a transition with this energy is observed.

We want to point out that, within the experimental accuracy, two energy levels have the same energies viz: 4849.4 keV and 4850.3 keV (fig. 2), respectively. The coincidence relationships, however, clearly show that there are two separate energy levels at approximately the same energy.

It could be remarked that, in spite of a maximum angular momentum input of 61 $\hbar$, we do not reach higher angular momenta than around 23 $\hbar$ in the observed level spin. There is, however, a number of levels with spin values in the range 19–20 $\hbar$ at the highest excitation energies observed spreading out the input γ flux.

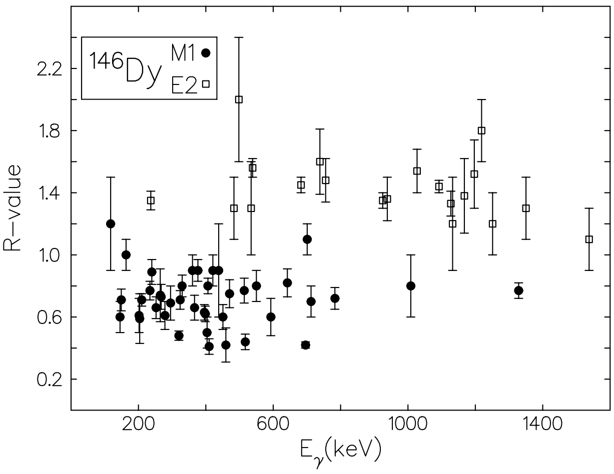

Fig. 4. Gamma-ray anisotropies, R (see text) plotted against the energies of a number of γ-ray transitions in ^{146}Dy.

4.2 Results for ^{147}Ho

Our results as regards the decay scheme of ^{147}Ho are shown in fig. 5. Also here a characteristic feature of the yrast scheme is complexity and an irregular structure. A few $\gamma\gamma$-coincidence spectra are shown in fig. 6. Table 2 gives the γ-ray energies, relative intensities and anisotropies. A number of R-values are plotted in fig. 7.

The main experimental problem in studying this nucleus is to find the missing transition from the 315 ns isomeric state. As suggested by Nolte *et al.* [4], the missing transition should be strongly converted and have an energy less than 60 keV. Probably, one is looking for a $27/2^- \rightarrow 23/2^- E2$ transition. Also in our study no such transition could be traced directly. The energy gap, however, could be searched for using the coincidence relationships of the γ cascades. A close study of the decays reveals an energy gap of 32 keV in the γ energy loops (fig. 5). A gap of this size corresponds well to the conclusions of Nolte *et al.* [4] mentioned above.

A characteristic feature of the yrast scheme shown in fig. 5 is a number of decay sequences, one of which, with direct transitions to the $27/2^-$ isomeric state at 2687 keV, extends to the highest spin value observed. Another part of the decay scheme has been interpreted as representing the positive-parity cascades, characterized by transitions to the two proposed $23/2^+$ states at 2469 and 2431 keV. The level scheme extends up to an excitation energy of about 8.7 MeV and a spin value of $53/2$ $\hbar$, *i.e.* we reach here somewhat higher values of angular momentum than in ^{146}Dy.

4.3 Results for ^{148}Er

The level scheme of ^{148}Er is shown in fig. 8. Table 3 gives the γ-ray energies, relative intensities and anisotropies, as well as the placement of the transitions in the level scheme. A plot of some R-values is given in fig. 9 and fig. 10 shows some coincidence spectra.

In the same way as for ^{146}Dy, also the level scheme of ^{148}Er can be divided in two parts. One part represents states at relatively low excitation energy (< 4.2 MeV) and low spin values ($\leq$12 $\hbar$) and with prompt decay to the ground state. The other part extends to high excitation energy ($\approx$ 9.6 MeV) and high spin values (23 $\hbar$) and the levels de-excite to the 10^+, 13 μs isomeric state at 2913 keV.

An important difference with respect to the level scheme of ^{146}Dy is that three 16^+ states are observed in ^{148}Er below an excitation energy of 6 MeV. In ^{146}Dy the yrast 16^+ state at 6093 keV is connected to the 10^+ isomeric state by a cascade of three $E2$ transitions. In ^{148}Er there is a 16^+ state at 5946 keV also connected to an isomeric 10^+ state by three $E2$ transitions. In addition to this 16^+ state, there are two 16^+ states in ^{148}Er situated at 5742 keV and 5304 keV. These additional 16^+ states are certainly associated with the two additional protons in ^{148}Er compared to ^{146}Dy. In ^{148}Er as well as in ^{146}Dy, a number of 17^- states are observed at an energy of about 6 MeV.

5 Discussion

The three $N = 80$ isotones ^{146}Dy,^{147}Ho and ^{148}Er can be described in the shell model as two neutron holes in the $h_{11/2}$, $s_{1/2}$, $d_{3/2}$ subshell and two, three and four protons, respectively, outside the inert core of ^{146}Gd. In these nuclei the Fermi level is close to the $h_{11/2}$ orbital for both neutrons and protons and consequently this orbital will dominate the high-spin yrast states.

Table 2. Gamma-ray energies, intensities and anisotropy ratios for γ-ray transitions in ^{147}Ho.

E_γ (keV)	I_γ	R	I_i^π ($\hbar$)	I_f^π ($\hbar$)
72.2(3)	11(2)		$19/2_1^+$	$19/2_2^-$
77.8(3)	66(6)	0.9(1)	$23/2_1^+$	$21/2^+$
80.5(2)	10(3)		$35/2_2^-$	$35/2_1^-$
103.5(4)	10(2)		$35/2_5^-$	$35/2_4^-$
115.9(1)	157(6)	0.68(4)	$23/2_2^+$	$21/2^+$
135.4(5)	67(4)	0.66(6)	$37/2_1^-$	$35/2_5^-$
139.2(1)	220(6)	0.63(3)	$41/2_2^-$	$39/2_3^-$
144.7(3)			$47/2_1^-$	$45/2_4^-$
150.3(3)[a]			$45/2_4^-$	$45/2_2^-$
150.7(3)[a]	47(5)		$35/2_5^-$	$35/2_3^-$
156.4(1)	64(5)	0.68(8)	$35/2_1^+$	$35/2_1^-$
165.2(2)	72(4)	0.65(6)	$21/2^+$	$19/2_2^+$
179.8(2)	36(3)	0.6(1)	$15/2^-$	$13/2^-$
185.6(3)	75(4)	0.63(6)	$49/2^-$	$47/2_1^-$
200.5(3)	18(3)		$45/2_1^+$	$43/2_3^+$
203.7(4)	39(4)	0.7(1)	$35/2_5^-$	$33/2_5^-$
224.6(2)	29(3)	0.7(1)	$27/2_1^+$	$25/2_3^+$
227.5(4)	40(3)	0.73(9)	$39/2_1^-$	$37/2_2^-$
238.0(3)	32(3)	0.8(1)	$37/2_1^-$	$35/2_4^-$
247.6(4)	30(3)	0.8(1)	$35/2_5^-$	$33/2_4^-$
253.5(2)	41(4)	0.9(1)	$37/2_2^-$	$35/2_4^-$
261.9(1)	70(4)	0.81(8)	$33/2_1^-$	$31/2_2^-$
274.0(2)	76(4)	0.82(8)	$43/2_1^+$	$41/2_3^+$
295.2(2)[a]	209(3)	0.98(3)	$35/2_2^-$	$33/2_1^+$
295.5(5)[a]			$35/2_5^-$	$33/2_3^-$
298.4(5)[a]	84(2)	0.85(4)	$21/2^+$	$19/2_1^+$
299.7(3)[a]			$35/2_7^-$	$35/2_4^-$
303.5(3)	20(2)	0.6(1)	$37/2_3^-$	$35/2_7^-$
315.5(7)	17(4)	0.6(2)	$31/2_1^+$	$29/2^+$
317.4(3)[a]	38(5)	0.71(9)	$45/2_1^+$	$43/2_1^+$
318.7(3)[a]			$19/2_1^+$	$19/2_1^-$
331.2(1)[a]	273(4)	0.79(2)	$39/2_3^-$	$37/2_3^-$
333.5(5)[a]			$27/2_1^+$	$25/2_2^+$
338.6(4)	12(4)		$43/2_1^+$	$41/2_2^+$
350.3(4)	33(4)		$43/2_2^+$	$41/2_3^+$
361.8(3)	22(3)	0.8(2)	$29/2_2^-$	$27/2_3^-$
366.5(4)	34(3)	2.5(7)	$33/2_1^+$	$33/2_1^-$
370.2(2)[a]			$21/2^+$	$19/2_2^-$
371.1(2)[a]	279(4)	0.79(2)	$35/2_1^+$	$33/2_1^+$
371.8(2)[a]			$43/2_1^-$	$41/2_2^-$
383.9(2)[a]	131(3)	1.18(6)	$33/2_1^-$	$31/2_1^-$
384.0(2)[a]			$37/2_1^+$	$35/2_1^+$
390.3(3)	49(2)	0.74(6)	$43/2_3^+$	$41/2_3^+$
397.6(4)	23(2)	0.6(1)	$27/2_1^+$	$25/2_1^+$
412.0(2)[a]	118(3)	0.89(5)	$41/2_3^+$	$39/2_3^+$
414.3(3)[a]	54(3)	0.91(7)	$41/2_1^+$	$39/2_2^+$
420.7(5)[a]	31(2)	0.59(7)	$41/2_2^+$	$39/2_2^+$
427.6(3)	10(2)		$33/2_4^-$	$31/2_4^-$
432.7(2)	48(3)	0.75(8)	$37/2_3^-$	$35/2_6^-$
435.7(3)	56(3)	0.85(9)	$31/2_3^-$	$29/2_2^-$
437.9(2)[a]			$41/2_1^-$	$39/2_1^-$
438.8(4)[a]	79(3)	0.89(6)	$39/2_2^+$	$37/2_3^+$
452.2(3)	12(2)		$19/2_2^+$	$19/2_1^-$
459.6(2)	49(2)	0.50(5)	$37/2_1^+$	$35/2_2^-$
463.8(4)[a]	37(3)	0.81(9)	$45/2_1^-$	$43/2_2^-$
465.5(4)[a]	80(3)	0.67(5)	$31/2_1^-$	$29/2_1^-$
471.8(5)[a]			$33/2_5^-$	$31/2_4^-$
472.2(4)[a]	37(3)	0.58(7)	$47/2^+$	$45/2_1^+$
481.5(2)[a]			$49/2^-$	$45/2_2^-$
481.8(2)[a]	148(3)	0.63(3)	$43/2_3^-$	$41/2_2^-$
491.2(4)	28(3)	0.5(1)	$41/2_3^-$	$39/2_2^-$
501.4(4)	37(3)	0.79(9)	$37/2_2^+$	$35/2_1^+$
509.3(4)[a]	67(3)	0.76(6)	$39/2_1^+$	$37/2_1^+$
509.5(7)[a]			$47/2_2^-$	$45/2_1^-$
512.5(4)[a]			$39/2_3^+$	$37/2_3^+$
514.6(3)[a]	47(3)		$19/2_1^+$	$15/2^+$
520.3(3)	106(3)		$37/2_3^+$	$35/2_1^+$
524.2(2)	43(3)	0.8(1)	$51/2^-$	$49/2^-$
553.3(4)	58(3)	0.67(6)	$39/2_2^-$	$37/2_1^-$
556.2(3)[a]	235(4)	0.72(2)	$25/2_1^+$	$23/2_2^+$
556.3(5)[a]			$53/2^-$	$51/2^-$
557.9(3)	32(3)	0.50(6)	$43/2_2^-$	$41/2_1^-$
567.5(2)	29(2)	0.52(7)	$45/2_3^-$	$43/2_3^-$
571.7(3)	35(2)	0.9(1)	$45/2_2^-$	$43/2_1^-$
575.7(2)	55(3)	0.67(6)	$39/2_2^+$	$37/2_1^+$
581.5(1)	137(3)	0.70(3)	$35/2_1^-$	$33/2_1^-$
585.0(2)[a]	214(3)	0.69(2)	$13/2^-$	$11/2^-$
588.0(2)[a]			$31/2_2^-$	$29/2_1^-$
594.2(3)[a]	25(2)	0.74(9)	$25/2_1^+$	$23/2_1^+$
596.5(5)[a]			$37/2_3^+$	$35/2_2^-$
617.5(1)	360(4)	0.98(9)	$21/2^+$	$19/2_1^-$
620.4(5)	53(2)	0.87(7)	$25/2_2^+$	$23/2_2^+$
628.6(3)	30(3)	1.57(24)	$33/2_1^+$	$31/2_2^-$
648.2(4)[a]			$19/2_2^+$	$15/2_2^+$
648.9(3)[a]	61(4)	0.87(8)	$39/2_3^+$	$37/2_1^+$
658.5(3)	40(2)	0.47(5)	$25/2_2^+$	$23/2_1^+$
661.6(2)[a]	173(3)	1.24(4)	$19/2_2^+$	$17/2_1^-$
661.9(2)[a]			$35/2_2^-$	$33/2_1^-$
701.0(1)	216(4)	0.9(2)	$37/2_3^-$	$35/2_2^-$
707.1(4)	25(2)	1.6(2)	$29/2^+$	$25/2_3^+$
728.8(1)	38(2)	0.72(7)	$25/2_3^+$	$23/2_2^+$
736.5(2)	50(2)	1.8(1)	$27/2_2^-$	$23/2^-$
741.6(3)	42(2)	1.4(1)	$27/2_3^-$	$23/2^-$
751.1(1)	157(4)	1.0(1)	$33/2_1^+$	$31/2_1^-$
755.0(9)	39(2)		$37/2_1^+$	$33/2_1^+$
762.2(3)[a]			$17/2^-$	$15/2^-$
764.7(1)[a]	1000(5)	1.43(2)	$15/2^-$	$11/2^-$
775.5(4)	60(3)	2.2(2)	$15/2^+$	$15/2^-$
783.5(2)	196(6)	1.6(1)	$33/2_1^+$	$29/2^+$
785.1(1)	355(6)	0.44(3)	$29/2_1^-$	$27/2_1^-$
798.1(1)	123(3)	1.64(6)	$31/2_1^+$	$27/2_1^+$
805.6(5)	13(2)		$21/2^-$	$19/2_1^-$
815.9(3)	92(3)	1.81(9)	$29/2^+$	$25/2_2^+$
850.1(1)	118(3)	1.1(1)	$33/2_1^-$	$29/2_1^-$
867.8(3)	64(3)	1.1(2)	$47/2_1^-$	$43/2_1^-$
880.1(1)	136(3)	1.64(7)	$29/2^+$	$25/2_1^+$
893.8(4)	36(2)	1.5(1)	$45/2_2^+$	$41/2_1^+$
903.6(5)[a]	28(2)	1.4(2)	$31/2_2^+$	$27/2_2^+$
903.8(5)[a]			$39/2_3^+$	$35/2_2^+$
918.9(2)	382(4)	1.52(3)	$23/2^-$	$19/2_1^-$
933.8(3)	48(2)	1.28(8)	$33/2_2^+$	$29/2^+$
941.7(2)	113(3)	1.40(5)	$17/2^-$	$13/2^-$
955.3(4)	61(4)	1.1(1)	$15/2^+$	$13/2^-$
969.0(3)[a]	103(4)	1.5(1)	$35/2_2^+$	$31/2_1^+$
971.1(2)[a]	825(5)	1.42(2)	$19/2_1^-$	$15/2^-$
976.4(4)	52(2)	1.07(6)	$33/2_3^+$	$29/2^+$
991.8(1)	105(3)	1.72(8)	$27/2_1^+$	$23/2_1^+$
1003.9(6)	24(2)	1.8(3)	$25/2_4^+$	$21/2^+$
1015.5(4)	22(2)	1.6(2)	$21/2^-$	$17/2^-$
1033.5(4)	42(3)	1.7(2)	$39/2_3^+$	$35/2_1^+$
1036.6(3)	34(2)	0.62(8)	$31/2_4^-$	$29/2_1^-$
1058.7(8)	30(3)	1.6(2)	$39/2_4^+$	$35/2_2^+$
1095.5(9)	15(3)		$35/2_3^-$	$31/2_1^-$
1104.7(6)	41(3)	2.2(2)	$39/2_4^-$	$35/2_4^-$
1144.0(3)	98(4)	1.31(9)	$35/2_4^-$	$31/2_1^-$
1146.3(5)	42(4)	1.6(3)	$41/2_4^-$	$37/2_1^-$
1210.1(9)	14(2)		$39/2_5^-$	$35/2_4^-$
1218.4(2)	70(2)	1.0(2)	$19/2_2^-$	$15/2^-$
1231.3(5)	28(2)	1.7(2)	$27/2_2^+$	$23/2_2^+$
1246.7(4)	48(2)	1.39(7)	$35/2_5^-$	$31/2_1^-$
1250.9(3)[a]	390(24)	1.53(3)	$31/2_1^-$	$27/2_1^-$
1251.1(9)[a]			$39/2_6^-$	$35/2_4^-$
1264.5(8)	13(2)		$27/2_3^+$	$23/2_2^+$
1267.5(8)			$43/2_4^-$	$39/2_6^-$
1293.6(8)	20(3)		$33/2_2^-$	$29/2_1^-$
1315.4(4)	33(2)	1.5(1)	$35/2_6^-$	$31/2_1^-$
1373.5(4)	97(2)	1.1(2)	$31/2_2^-$	$27/2_1^-$
1416.6(5)	17(2)	1.9(4)	$33/2_3^-$	$29/2_1^-$
1444.0(7)	12(2)		$35/2_7^-$	$31/2_1^-$

[a] Not resolved

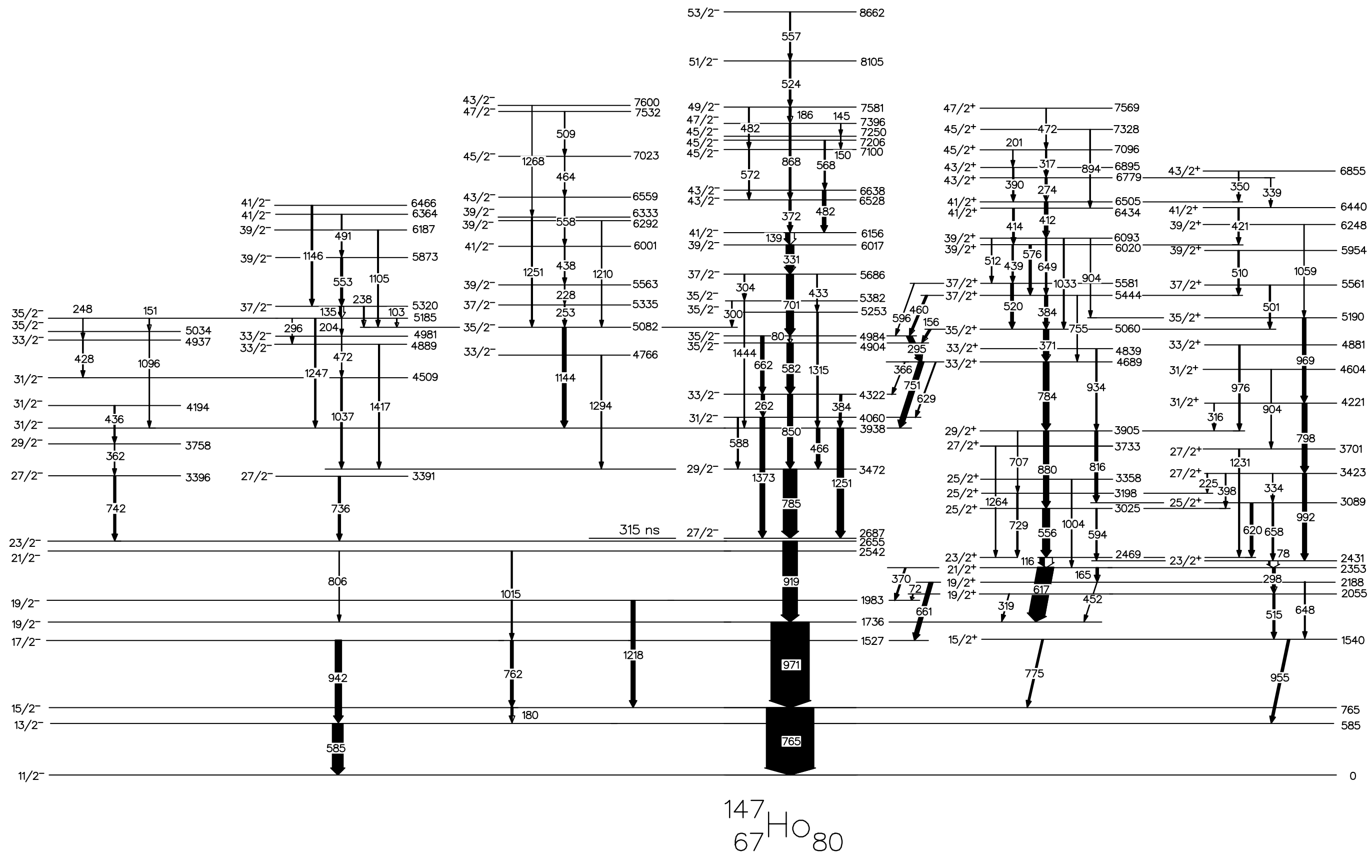

Fig. 5. Level scheme of ^{147}Ho deduced from the present work. The widths of the arrows are roughly proportional to the relative γ-ray intensities. Energies are given in keV.

5.1 ^{146}Dy and ^{148}Er

5.1.1 Low-lying positive-parity states

The 2^+ and 4^+ states in ^{146}Dy and ^{148}Er are clearly neutron two-quasiparticle (2qp) states. The 2^+ and 4^+ states in the $N = 82$ Dy and Er isotones come much higher, while the energies of the 2^+ and 4^+ levels in the $N = 80$ Gd, Dy and Er isotones are quite regular (fig. 11).

The 6_1^+ states are not uniquely identified as proton or neutron states. They could be $\pi h_{11/2}^2$ states, but they are 100–200 keV lower relative to the $(\pi h_{11/2}^2)$ 10^+ state than in the $N = 82$ nuclei. They could also be neutron states with a substantial $\nu d_{5/2}^{-1} \nu g_{7/2}^{-1}$ component.

The 8_1^+ states are probably also proton $h_{11/2}^2$ states, but they behave irregularly in comparison with the $N = 82$ isotones. In ^{148}Dy and ^{150}Er the 8^+ states come 86 keV and 63 keV below the 10^+ states, respectively. In contrast, the 8^+ state in ^{146}Dy comes above the 10^+ state ($t_{1/2}$=150 ms excludes $E2$ from 10^+ to 8^+), while in ^{148}Er the 8^+ state comes 131 keV below the 10^+ state.

The 10^+ isomeric states are clearly proton $h_{11/2}^2$ states. The neutron $(\nu h_{11/2}^{-2})10^+$ states in ^{146}Dy and ^{148}Er are expected around 3.7 MeV according to systematics from lighter $N = 80$ nuclei [13].

5.1.2 Low-lying negative-parity states

Several of the negative-parity states from 3^- to 9^- in ^{146}Dy and ^{148}Er are proton 2qp states. Two β-decay experiments have identified some of these states in the $N = 82$ isotones of Dy and Er [14,15]. In table 4 some identifications are suggested. The missing 3^- state in ^{148}Er should come at about 1850 keV. The reason that it is not observed to be populated from 5^- state in ^{148}Er as in ^{146}Dy is simply a matter of intensity branching.

One can also identify the states $(\nu s_{1/2}^{-1} \nu h_{11/2}^{-1})5^-$ and $(\nu d_{3/2}^{-1} \nu h_{11/2}^{-1})7^-$ by comparison with ^{144}Gd (table 5). The variation of energy with Z is very regular.

The 3898 keV (10^-) and 4194 keV (11^-) levels in ^{146}Dy are most probably 4qp states, coupling $\nu(2^+$, 682 keV) to $\pi(8^-$, 3159 keV) and $\pi(9^-$, 3438 keV), respectively. The equivalent states in ^{148}Er are unobserved.

5.1.3 Four-quasiparticle states (4qp) of positive parity feeding into the isomeric 10^+ state

The strongly excited 11^+ states 3632 keV (^{146}Dy), 3528 keV (^{148}Er) and 12^+ states 4028 keV (^{146}Dy), 3723 keV (^{148}Er) are unique and clearly all of the configuration $(\pi h_{11/2}^2;10^+)\otimes(\nu s_{1/2}^{-1} d_{3/2}^{-1};2^+)$. In ^{144}Gd$_{80}$ the

Table 3. Gamma-ray energies, intensities and anisotropy ratios for γ-ray transitions in ^{148}Er.

E_γ (keV)	I_γ	R	I_i^π ($\hbar$)	I_f^π ($\hbar$)	E_γ (keV)	I_γ	R	I_i^π ($\hbar$)	I_f^π ($\hbar$)
110.5(2)	79(4)	0.50(7)	15_2^-		615.7(2)[a]	419(7)	0.56(2)	11^+	10^+
131.2(2)			10^+	8^+	616.1(3)[a]				20_3^+
145.3(3)	44(4)	0.65(5)	(21^+)	(20^+)	631.2(2)	76(5)	1.1(1)	(20^-)	19_2^-
150.4(3)			15_2^-	14^-	645.9(1)	280(7)	1.42(7)	2^+	0^+
168.8(1)	87(8)	2.1(7)	7_2^-	7_1^-	650.7(2)	68(5)	2.2(3)		7_2^-
194.4(1)	73(5)	0.64(9)	12^+	11^+	729.8(1)	193(7)	0.96(7)	5^-	4^+
201.9(1)	181(7)	0.65(5)	17_4^-	16_2^-	739.9(3)	58(5)	1.5(2)	19_1^-	17_3^-
203.8(2)			16_3^+	16_2^+	798.9(4)	119(6)	0.35(9)	17_1^+	16_1^+
211.9(1)	142(6)	0.75(6)	19_1^+	18_3^+	801.9(2)	118(5)	1.4(1)	19_2^-	17_4^-
242.0(2)	48(40	0.8(1)	18_2^+	17_2^+	808.0(2)[a]			19_1^-	17_2^-
256.8(2)[a]			(22^-)	21_1^-	809.4(4)[a]			13^+	12^+
257.1(2)[a]	140(17)	0.9(2)	8^+	6^+	810.1(1)[a]	1741(15)	1.43(2)	12^+	10^+
274.4(1)	165(6)	0.84(7)	(23^-)	(22^-)	819.2(2)[a]			16_3^+	14_2^+
282.6(2)	139(6)	1.3(1)	7_1^-	5^-	819.5(1)[a]	77(5)	2.0(3)		
284.7(2)	37(5)	0.5(2)	19_1^+	18_2^+	839.8(1)	104(5)	1.4(1)	19_1^-	17_1^-
299.9(1)	73(5)	0.8(1)	21_1^+	20_2^+	876.8(1)	240(6)	1.44(7)	4^+	2^+
305.1(1)	417(7)	1.28(4)	15_1^-	13^-	885.9(2)	94(7)	1.1(2)	12^-	12^+
314.8(1)	179(6)	0.86(5)	18_3^+	17_2^+	948.4(2)	71(4)	2.1(3)	20_3^+	18_2^+
343.5(1)	80(6)	1.0(1)	17_4^-	16_3^+	955.0(1)	501(8)	1.01(3)	13^-	12^+
345.5(3)[a]			16_2^-	16_2^+	969.1(4)	31(5)			
346.9(1)[a]	193(7)	0.70(5)	18_2^+	17_4^-	981.1(1)	1000(7)	1.60(3)	14_1^+	12^+
381.8(4)	100(7)	0.8(1)	19_2^-	18_3^+	990.6(1)	180(5)	1.50(8)	21_1^-	19_1^-
385.6(4)	41(7)	1.2(4)	17_2^+		1002.4(2)[a]			6^+	4^+
393.0(3)	38(7)	1.5(6)	14^-	14_1^+	1003.1(3)[a]	336(7)	1.56(6)	13^+	11^+
399.5(2)	84(8)	0.7(1)	(19^+)	(18^+)	1027.9(2)	80(4)	1.8(2)	21_2^-	19_2^-
415.4(3)	68(7)	0.7(1)	18_1^+	17_1^+	1038.1(2)	250(6)	1.45(7)	16_2^+	14_1^+
432.6(1)	167(7)	0.78(6)	20_1^+	19_1^+	1041.6(3)	72(4)	1.6(2)		(23^-)
438.6(3)	75(6)	0.9(1)	(20^+)	(19^+)	1054.7(3)	58(5)			16_1^-
448.5(1)	246(7)	0.91(5)	17_2^+	16_3^+	1080.5(4)	80(5)	0.88(9)	12^-	11^+
451.4(1)[a]			7_2^-	5^-	1104.5(3)	163(5)	0.86(6)	16_2^-	15_1^-
451.8(2)[a]	117(5)	1.00(9)			1152.4(2)[a]				18_1^+
454.8(2)	59(5)	0.36(8)	19_2^-	18_2^+	1152.7(3)[a]	159(8)		(18^+)	16_2^+
459.2(2)	74(6)	1.0(2)		13^-	1185.9(3)	31(3)	2.1(4)	23^+	21^+
467.3(1)[a]				7_2^-	1204.3(2)	45(4)	1.2(2)	17_1^-	15_1^-
467.4(1)[a]	289(7)	0.85(5)	16_1^-	15_2^-	1214.3(1)	148(5)	1.52(9)	18_1^+	16_1^+
471.8(2)	98(6)	0.78(9)	17_1^-	16_1^-	1235.4(2)	90(5)	1.3(1)	17_2^-	15_1^-
480.9(1)	141(12)	0.45(9)	20_2^+	19_2^+	1242.0(1)	342(6)	1.48(5)	16_3^+	14_1^+
488.1(3)			14^-	12^-	1252.4(3)	178(6)	0.89(6)		19_2^+
503.3(2)	130(9)	0.9(1)	17_2^-	16_1^-	1304.1(4)[a]	150(5)	1.59(9)		15_1^-
533.2(1)	171(8)	0.66(7)	19_2^+	18_1^+	1304.9(4)[a]				14_1^+
565.8(1)	177(8)	0.91(8)	14^-	13^+	1404.3(4)	42(3)	1.5(2)	14_2^+	12^+
599.6(1)	374(7)	1.60(6)	16_1^+	14_1^+					

[a] Not resolved

$\nu s_{1/2}^{-1} d_{3/2}^{-1}; 2^+$ state comes at 743 keV. Due to the $\pi\nu$ interaction 11^+ is shifted down 47 keV, 12^+ is shifted up by 349 keV in ^{146}Dy. The energy splitting between the 11^+ and 12^+ states decreases from 396 keV in Dy to 195 keV in Er. This decrease is interpreted as an effect of the quadrupole-quadrupole coupling, which becomes less effective in Er because the quadrupole moment of $\pi(10^+)$ is smaller in Er due to the increased filling of the $\pi h_{11/2}$ shell. A related effect is seen in the decreasing $B(E2)'$s for $10^+ \to 8^+$ in $N = 82$ isotones [16].

Similarly, the 13^+ states 4850 keV (^{146}Dy), 4532 keV (^{148}Er) and 14^+ states 5155 keV (^{146}Dy), 4704 keV (^{148}Er) are naturally interpreted to correspond to the $(\pi h_{11/2}^2;10^+)\otimes(\nu d_{3/2}^{-1} d_{5/2}^{-1};4^+)$ configuration. The 4_1^+ state in ^{144}Gd$_{80}$ at 1744 keV must be mainly a neutron 2qp $d_{3/2}^{-1} d_{5/2}^{-1}$ state, since the proton 4_1^+ state in ^{146}Gd$_{82}$ comes much higher, at 2612 keV. The $\pi\nu$ interaction is now +170 keV in 13^+, +475 keV in 14^+ for ^{146}Dy. Also here the splitting between 13^+ and 14^+ decreases from 305 keV in Dy to 172 keV in Er, and the reason is probably the same as stated above.

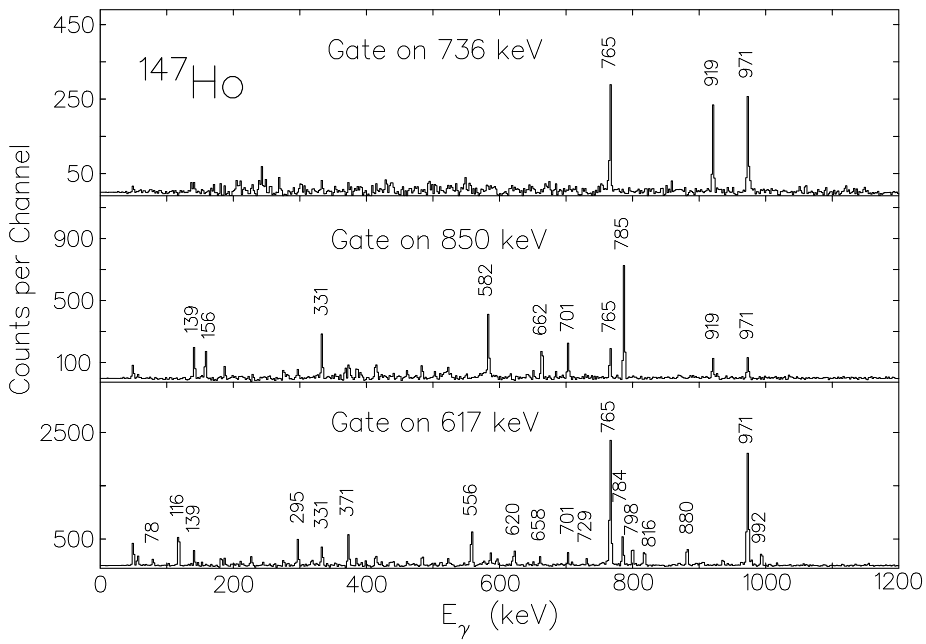

Fig. 6. Some background-subtracted $\gamma\gamma$-coincidence spectra of ^{147}Ho recorded with NORDBALL. Only the most prominent γ-rays are indicated.

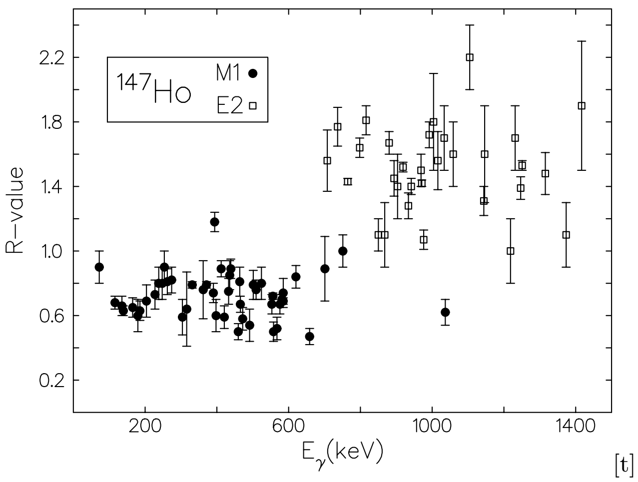

Fig. 7. Gamma-ray anisotropies, R (see text) plotted against the energies of a number of γ-ray transitions in ^{147}Ho.

Table 4. Proton 2qp states (energies in keV).

I^π	^{146}Dy	^{148}Dy [14]	^{148}Er	^{150}Er [15]
9^-	3438	-	-	-
8^-	(3338)	(3405)	(3355)	-
8^-	3159	-	-	-
7^-	2806	2739	2704	2633
5^-	2280	2350	2253	2260
3^-	1782	1688	-	1786

In ^{148}Dy$_{82}$ positive-parity states with spin values 12^+ and 14^+ are known at 4851 keV and 5410 keV, respectively. These states must be proton states, corresponding to the coupling of $(\pi h^2_{11/2})10^+$ to the ^{146}Gd$_{82}$ particle-hole states 2^+ (1972 keV) and 4^+ (2612 keV). In ^{146}Dy the 14^+_2 state at 5378 keV most probably is the same proton state as 14^+ (5410 keV) in ^{148}Dy. The decay of the 14^+_2 state in ^{146}Dy by a γ transition of 118 keV to 13^+_2 (5260 keV) shows that this state is also of the type $(\pi h^2_{11/2})10^+ \otimes (\pi\pi^{-1})4^+$.

Table 5. Neutron 2qp states (energies in keV).

I^π	^{144}Gd [13]	^{146}Dy	^{148}Er
7^-	2471	2517	2535
5^-	2442	(2458)	-

Table 6. Energy spacings to the 10^+ states compared to the 3^- energy (energies in keV).

	$N = 82$	$N = 80$
11^- - 10^+ (Dy)	1061	1328
12^- - 10^+ (Dy)	1557	1538
3^- (Gd)	1579	1702
11^- - 10^+ (Er)	1204	-
12^- - 10^+ (Er)	1681	1696
3^- (Dy)	1688	1782

Table 7. Energy spacings to the 10^+ states (energies in keV).

	^{150}Er	^{148}Er
13^- - 10^+	1694	1765
15^- - 10^+	2088	2070
16^+ - 10^+	2425	2390

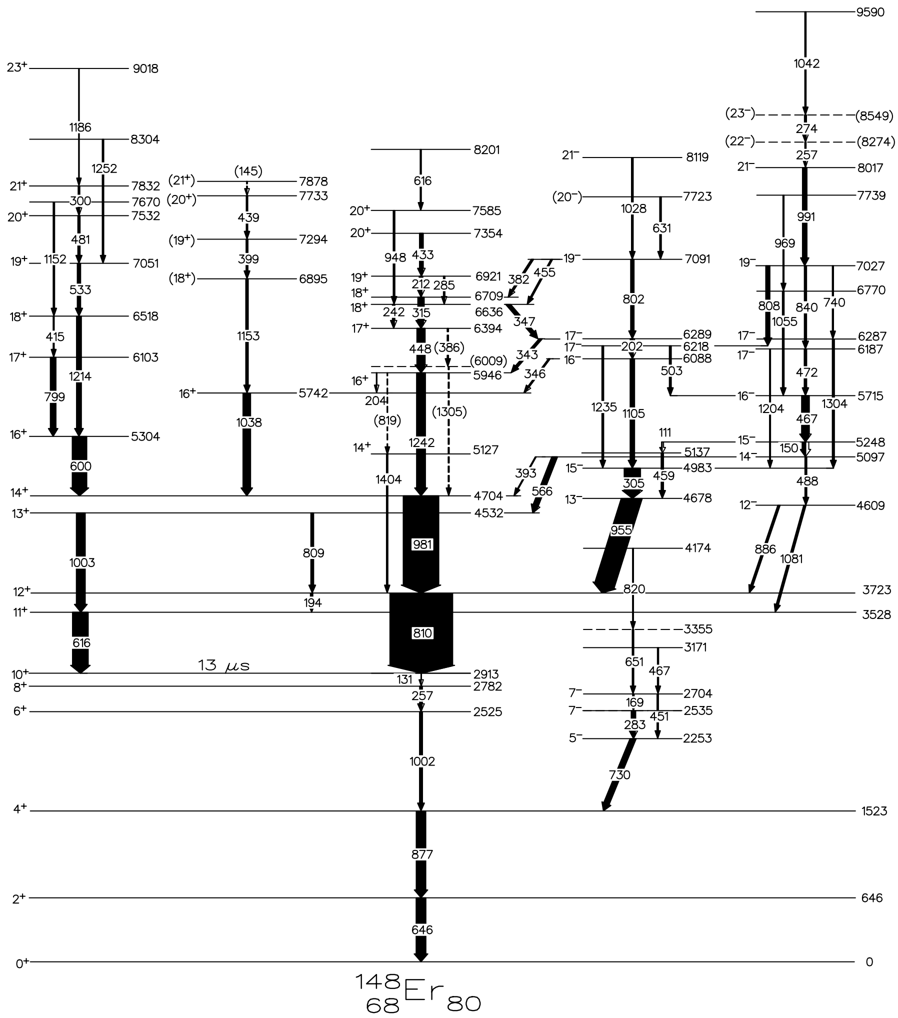

Fig. 8. Level scheme of ^{148}Er. The widths of the arrows are roughly proportional to the relative γ-ray intensities. Energies are given in keV.

5.1.4 Four-quasiparticle proton states of negative parity

The lowest states of this kind are $\pi h^2_{11/2} \otimes 3^-$, where 3^- is a particle-hole excitation, mostly of a proton. The 11^- and 12^- states of this type are known both in $^{148}Dy_{82}$ and $^{150}Er_{82}$. In table 6 the energies from 10^+ up to 11^- or 12^- are compared with the 3^- energy. The $N = 82$ energies are well understood in terms of a large $\pi h_{11/2} d^{-1}_{5/2}$ component in 3^- state. The $N = 80$ energies are in line with this interpretation. We are therefore convinced that 11^- (4264 keV), 12^- (4474 keV) in ^{146}Dy and 12^- (4609 keV) in ^{148}Er are such octupole states.

The $\pi h^2_{11/2} \otimes 3^-$ maximum-spin state 13^- is pushed up a lot in energy by the effect of the Pauli principle on the $\pi h_{11/2} d^{-1}_{5/2}$ component in 3^-. In ^{146}Dy it may be one of the experimental 13^- states at 4849 keV or 5066 keV.

States of the type $\pi h^3_{11/2}(\pi d^{-1}_{5/2}$ or $\pi g^{-1}_{7/2})$ with spin 14^-, 16^-, 17^- are well known in ^{148}Dy. A numerical calculation using as far as possible empirical matrix elements gives the corresponding 16^-, 17^- states in ^{146}Dy to come at 5920 keV and 6200 keV, respectively, and they may be identified with the levels at 5933 keV (16^-) and 6260 keV (17^-). An alternative could be the states at 6116 keV (16^-) and 6325 keV (17^-). However, there is at the moment nothing but the energy agreement which favours

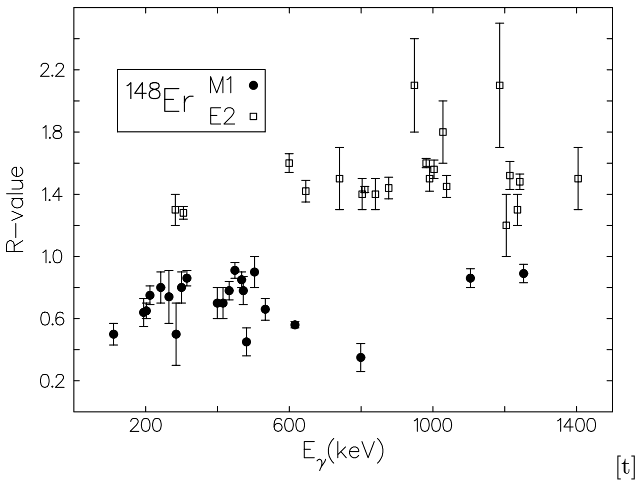

Fig. 9. Gamma-ray anisotropies, R (see text) plotted against the energies of a number of γ-ray transitions in ^{148}Er.

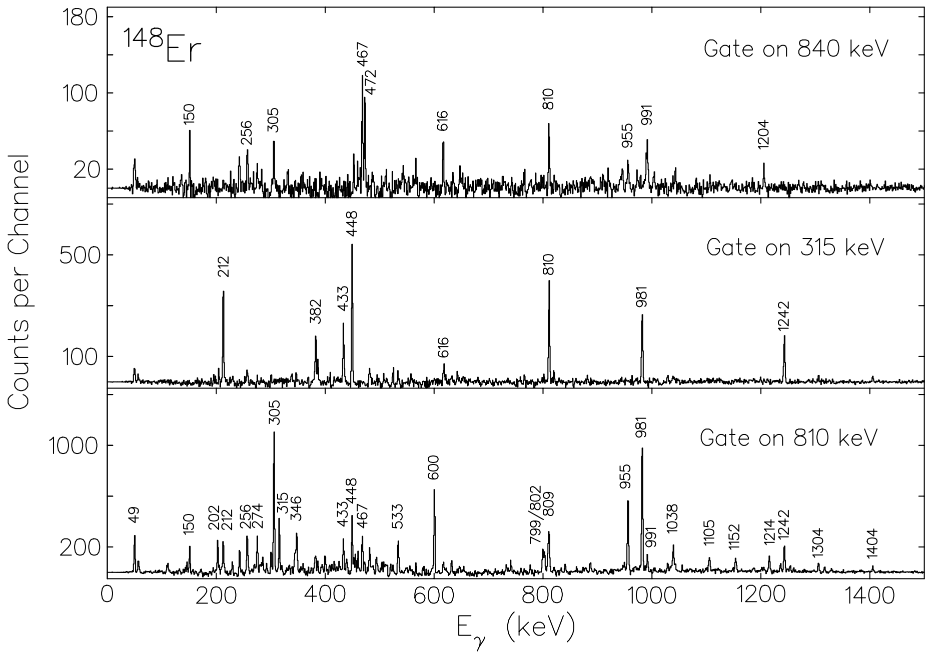

Fig. 10. Some back- ground-subtracted $\gamma\gamma$-coincidence spectra of ^{148}Er recorded with NORDBALL. Only the most prominent γ-rays are indicated. Note that the 810 keV gating transition is a doublet ($12^+ \rightarrow 10^+$ and $13^+ \rightarrow 12^+$).

Table 8. Matrix elements (keV) used for the calculation of energies of the configuration $\pi h_{11/2}^2 \nu d_{3/2}^{-1} \nu h_{11/2}^{-1}$ in ^{146}Dy.

I^π	$\pi h_{11/2} \nu d_{3/2}^{-1}$	$\nu d_{3/2}^{-1} \nu h_{11/2}^{-1}$
7^-	+370	−380
6^-	+20	0
5^-	0	0
4^-	+400	0

these identifications. The analogous 4qp states in ^{150}Er with a proton hole $d_{5/2}^{-1}$ or $g_{7/2}^{-1}$ are not known. The levels in ^{148}Er at 6088 keV (16^-) and 6289 keV (17^-) might be these states.

In the $N = 82$ nucleus ^{150}Er there are also known 4qp proton states, *i.e.* $(\pi h_{11/2}^3 \pi s_{1/2})13^-$ at 4491 keV, $(\pi h_{11/2}^3 d_{3/2})15^-$ at 4885 keV and $(\pi h_{11/2}^4)16^+$ at 5222 keV. The equivalent 16^+ state in ^{148}Er is definitely the level at 5304. It is also quite likely that the experimental levels at 4678 keV (13^-) and 4983 keV (15^-) in ^{148}Er are these states. The energy spacings to the 10^+ state agree quite well (table 7). The 305 keV ($15^- \rightarrow 13^-$) $E2$ transition in ^{148}Er is a fast single-particle $d_{3/2} \rightarrow s_{1/2}$ transition, same as in ^{150}Er.

Table 9. Candidates for 13^-, 14^-, 15^-, 16^- and 17^- yrast states of the type $\pi h_{11/2}^2 \nu d_{3/2}^{-1} \nu h_{11/2}^{-1}$ (energies in keV).

I^π	^{146}Dy (calc.)	^{146}Dy	^{148}Er
17^-	6230	6260	6187 or 6218
16^-	5740	5743	5715
15^-	5240	5333 or 5419	5248
14^-	5050	5013 or 5270	5097 or 5137
13^-	4990		

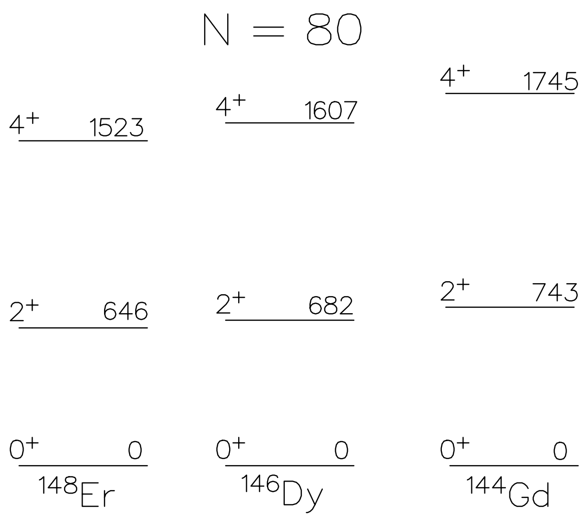

Fig. 11. Energies of 2^+ and 4^+ states of the $N = 80$ isotones of ^{144}Gd, ^{146}Dy and ^{148}Er.

5.1.5 Yrast and near-yrast states

There should be a host of yrast or near-yrast 4qp states with negative parity of the type: $\pi h_{11/2}^2(10^+) \otimes \nu(s_{1/2}^{-1}$ or $d_{3/2}^{-1})\nu h_{11/2}^{-1}$. A numerical calcula-

Table 10. Matrix elements (keV) used for the calculation of energies of the configuration $\pi h^2_{11/2}\nu h^{-2}_{11/2}$ in ^{146}Dy.

$\pi h^2_{11/2}$	$\pi h_{11/2}\nu h^{-1}_{11/2}$	$\nu h^{-2}_{11/2}$
10^+ +320	11^+ +650	10^+ +120
8^+ +230	10^+ + 60	8^+ + 30
6^+ +130	9^+ +100	6^+ − 70
	8^+ +100	
	7^+ +150	
	6^+ +150	
	5^+ +200	
	4^+ +250	

Table 11. Identification of the sequence of 4qp yrast states of the type $\pi h^2_{11/2} \otimes \nu h^{-2}_{11/2}$ (energies in keV).

I^π	^{146}Dy (calc.)	^{146}Dy	^{148}Er
20^+	7480	unobserved	7354
19^+	7080	7189	6921
18^+_a	6820	6924	6709
18^+_b	6740	6893	6636
17^+	6520	6564	6394
16^+	6070	6093	5946

tion of the $\pi h^2_{11/2}\nu d^{-1}_{3/2}\nu h^{-1}_{11/2}$ states in ^{146}Dy using empirical interaction matrix elements according to table 8 gives candidates for all states from 13^- to 17^- and in combination with the ^{148}Er data the identification given in table 9 is suggested.

The 4qp states of the type $\pi h^2_{11/2}\otimes\nu h^{-2}_{11/2}$ were also calculated (for matrix elements see table 10). The whole sequence 16^+, 17^+, 18^+_a, 18^+_b, 19^+, 20^+, connected by $M1$ transitions, is very probable seen in ^{148}Er. With that in hand the identification of these states in ^{146}Dy up to 19^+ is strengthened (table 11). The calculated position of the 16^+ state is 6070 keV in close agreement with the measured value of the yrast 16^+ state in ^{146}Dy at 6093 keV. The energy agreement is so good that an adjustment of the matrix elements is not justified.

5.1.6 Six-quasiparticle states (6qp)

There are clearly many observed levels above 5 MeV in both nuclei, which cannot be of 2qp or 4qp nature. Some of these levels appear at energies where 6qp states are expected. As an example, many levels in the group of negative-parity levels in ^{146}Dy between 5.0 and 5.6 MeV are probably $\pi h^2_{11/2}\otimes\pi(3^-)\otimes\nu(2^+)$ and $\pi h^2_{11/2}\otimes\pi(3^-)\otimes\nu(4^+)$ states. Similarly, many of the higher negative-parity levels with spins 16–21 may be 6qp states, coupling $\pi(h^3_{11/2}d^{-1}_{5/2})$ or $\pi(h^3_{11/2}g^{-1}_{7/2})$ to the low-lying $\nu(2^+)$ or $\nu(4^+)$ excitations. If the 17^- level in ^{148}Er at 6289 keV is the highest-spin state of the $\pi(h^3_{11/2}g^{-1}_{7/2})$ configuration, as suggested above, then the feeding indicates that the 19^-(7091 keV), 20^- (7723 keV) and 21^- (8119 keV) levels have the same proton structure, combined with the $\nu(2^+)$ or $\nu(4^+)$ excitations. In general, however, because of the high density of levels, and consequently expected mixing of different structures, it is not possible to assign 6qp configurations to individual levels.

Table 12. Comparison of some π^3 states in ^{149}Ho [17] and ^{147}Ho (energies in keV).

Proton configuration	I^π	$E(^{149}$Ho)	$E(^{147}$Ho)
$h^2_{11/2}s_{1/2}$	$19/2^+$	2025	2055
$h^2_{11/2}d_{3/2}$	$23/2^+$	2409	2431 or 2469
$h^3_{11/2}$	$23/2^-$	2593	2655
$h^3_{11/2}$	$27/2^-$	2737	2687

Table 13. Identification of $\pi h^n_{11/2}\otimes\nu(2^+)$ and $\pi h^n_{11/2}\otimes\nu(4^+)$ states, see text (energies in keV).

	^{146}Dy	^{147}Ho	^{148}Er
$\nu(2^+)$	696 (11^+-10^+)	785 ($29/2^-$-$27/2^-$)	799 (17^+-16^+)
	1092 (12^+-10^+)	1251 ($31/2^-$-$27/2^-$)	1214 (18^+-16^+)
$\nu(4^+)$	1914 (13^+-10^+)	1635 ($33/2^-$-$27/2^-$)	1748 (19^+-16^+)
	2219 (14^+-10^+)	2217 ($35/2^-$-$27/2^-$)	2229 (20^+-16^+)

5.2 Levels in ^{147}Ho

Starting with 3qp states, the $13/2^-$ (585 keV) and $15/2^-$ (765 keV) levels are clearly $\pi h_{11/2}\otimes\nu^{-2}(2^+)$ states analogous to the yrast 11^+ and 12^+ levels in ^{148}Er. The splitting is 180 keV in ^{147}Ho, 195 keV in ^{148}Er.

The $17/2^-$(1527 keV) and $19/2^-$(1736 keV) levels are probably $\pi h_{11/2}\otimes\nu^{-2}(4^+)$ states, to be compared with 13^+(4532 keV) and 14^+(4704 keV) in ^{148}Er. The splitting is 209 keV in ^{147}Ho and 172 keV in ^{148}Er.

The π^3 states with configurations $h^2_{11/2}s_{1/2}$, $h^2_{11/2}d_{3/2}$ and $h^3_{11/2}$ are known in ^{149}Ho [17] and similar states can also be found in ^{147}Ho (table 12). In all four cases the energies agree to better than 100 keV. The only realistic interpretation of the second $23/2^+$ level is $\pi h_{11/2}\otimes\nu^{-2}(7^-)$. The half-life 315 ns for the $27/2^-$ state of the $h^3_{11/2}$ configuration at 2687 keV gives $B(E2) = 2.7$ W.u., as expected somewhat larger than the value $B(E2) = 1.9$ W.u. for the corresponding transition in ^{149}Ho.

States of the type $\pi h_{11/2} \otimes \nu h_{11/2}^{-2}$ and analogous to the $h_{11/2}^2 \otimes h_{11/2}^{-2}$ sequences $16^+ \rightarrow 20^+$ can be suggested:

$$31/2^-(4194\ \text{keV}),$$
$$29/2^-(3758\ \text{keV}),$$
$$27/2^-(3396\ \text{keV}).$$

Interpolating between ^{146}Dy and ^{148}Er, some 5qp states above $27/2^-(2687$ keV) can be suggested (table 13). Here, some states of configurations $\pi h_{11/2}^3 \otimes \nu^{-2}(2^+$ or $4^+)$ in ^{147}Ho are compared with similar states in ^{146}Dy and ^{148}Er, containing 2 or 4 protons in the $h_{11/2}$ shell, respectively.

Some higher 5qp states can be considered above 5 MeV, but the complexity of the experimental level scheme makes it difficult to perform positive identifications. There is, however, one more ^{147}Ho level, which has a reasonably clear interpretation, *i.e.* $29/2^+$ (3905 keV). This state is $\pi h_{11/2}^3 \otimes 3^-$. A sequence of levels $35/2^+$ - $37/2^+$ - $39/2^+$ - $41/2^+$ is expected with the highest spin value originating from a parallel coupling of the structure $\pi(27/2^-) \otimes \nu(7^-)$. The $41/2^+$ state could be one of the levels at 6434 keV or 6505 keV.

6 Summary

From the preceding discussion it is evident that the three $N = 80$ isotones ^{146}Dy, ^{147}Ho and ^{148}Er can be well described by the spherical shell model indicating a predominantly spherical shape at the excitation energies and angular momenta reached in the present work.

The authors are grateful to the staff of the Niels Bohr institute, Risø, for their hospitality and for providing beams and technical support. We are especially indebted to J. Westergaard for operating the NBI Tandem van de Graaff and booster system. The authors gratefully acknowledge E. Ideguchi for technical help with the Si ball and A. Nilsson for help during the measurements. The support from the Swedish Natural Science Research Council (NFR) is greatly appreciated.

References

1. P. Kleinheinz, R. Broda, P.J. Daly, S. Lunardi, M. Ogawa, J. Blomqvist, Z. Phys. A **290**, 279 (1979).
2. S.Z. Gui, G. Colombo, E. Nolte, Z. Phys. A **305**, 297 (1982).
3. G. de Angelis, D. Bazzacco, S. Beghini, A.M. Bizzeti-Sona, P.G. Bizzeti, M.A. Cardona, L. Corradi, A. Dassie, A. D'Onofrio, M. De Poli, S. Lunardi, H. Moreno, L. Muller, D.R. Napoli, G. Nardelli, J. Rico, V. Roca, G.F. Segato, C. Signorini, F. Soramel, P. Spolaore, A.M. Stefanini, F. Terrasi, Z. Phys. A **341**, 371 (1992).
4. E. Nolte, G. Colombo, S.Z. Gui, G. Korschinek, W. Schollmeier, P. Kubik, S. Gustavsson, R. Geier, H. Morinaga, Z. Phys. A **306**, 211 (1982).
5. E. Nolte, S.Z. Gui, G. Colombo, G. Korschinek, K. Eskola, Z. Phys. A **306**, 273 (1982).
6. F. Pühlhofer, Nucl. Phys. A **280**, 267 (1977).
7. B. Herskind, Nucl. Phys. A **447**, 395c (1985).
8. S.E. Arnell, T. Kuroyanagi, S. Mitarai, J. Nyberg, H.A. Roth, Ö. Skeppstedt, *The NORDBALL system adapted for spectroscopy of nuclei far from stability* in *Proceedings of the Nuclear Physics in the Nineties* Vol. 1 (Oak Ridge National Laboratory, Oak Ridge, Tennessee, 1990) p. 214.
9. S.E. Arnell, H.A. Roth, Ö. Skeppstedt, J. Białkowski, M. Moszyński, D. Wolski, J. Nyberg, Nucl. Instr. Meth. A **300**, 301 (1991).
10. T. Kuroyanagi, S. Mitarai, S. Suematsu, B.J. Min, H. Tomura, J. Mukai, T.T. Maeda, R. Nakatani, G. Sletten, J. Nyberg, D. Jerrestam, Nucl. Instr. Meth. A **316**, 289 (1992).
11. S.E. Arnell, D. Foltescu, H.A. Roth, Ö. Skeppstedt, J. Blomqvist, A. Nilsson,T. Kuroyanagi, S. Mitarai, J. Nyberg, Phys. Rev. C **49**, 51 (1994).
12. D.C. Radford, Nucl. Instr. Meth. A **361**, 297 (1995).
13. M. Lach, J. Styczen, R. Julian, M. Piiparinen, H. Beuscher, P. Kleinheinz, J. Blomqvist, Z. Phys. A **319**, 235 (1984).
14. J.L. Tain, B. Rubio, P. Kleinheinz, D.Schardt, R. Barden, J. Blomqvist, Z. Phys. A **333**, 29 (1989).
15. A. Gadea, B. Rubio, J.L. Tain, J. Rico, J. Bea, L.M. Garcia-Raffi, P. Kleinheinz, D. Schardt, E. Roecki, R. Kirchner, J. Blomqvist, Z. Phys. A **355**, 253 (1996).
16. J.H. McNeill, J. Blomqvist, A.A. Chishti, P.J. Daly, W. Gelletly, M.A.C. Hotchkis, M. Piiparinen, B.J. Varley, P.J. Woods, Phys. Rev. Lett. **63**, 860 (1989).
17. J. Wilson, S.R. Faber, P.J. Daly, I. Ahmad, J. Berggreen, P. Chowdhury, T.L. Khoo, R.D. Lawson, R.K. Smither, J. Blomqvist, Z. Phys. A **296**, 185 (1980).